Publications

Available Online

J. Sci. Res. **17** (2), 377-391 (2025)

JOURNAL OF SCIENTIFIC RESEARCH

www.banglajol.info/index.php/JSR

Pentagonal Shaped Fractal Band Notch Antenna using Parasitic Notch Filter

P. Shinde[1*], J. Shinde[2]

[1]Department of E & TC, Bhivarabai Sawant College of Engineering & Research, Pune, Maharashtra-411041, India

[2]Department of E &TC, Sinhgad Academy of Engineering, Pune, Maharashtra-411048, India

Received 19 June 2024, accepted in final revised form 4 February 2025

Abstract

This paper presents the design of a band-notched simple iterative compact pentagonal fractal antenna. The antenna dimensions are W × L = 32 mm × 22 mm. The fractal radiating patch is placed on the front side of the FR 4 substrate material. The proposed fractal antenna geometry consists of a pentagon shape with three simple iterations of scale factor 0.62. The band-notched filter has been achieved by itching the pentagon shape as a parasitic patch on the back side of the substrate. The impedance bandwidth and reflection coefficient of the antenna are improved with the design of three iterations. The experimental results of the proposed CPW feed fractal antenna demonstrate wide band performance of 8.73 GHz ranging from 2.78 GHz to 11.51 GHz except the notched band frequency and exhibit peak gain of 8 dBi. The electromagnetically coupled pentagon parasitic patch is effectively optimized with respect to side length and position for notch-band development at 5.6 GHz, 9.3 GHz, and 12.5 GHz. These notch bands reject the interference of the 802.11a WLAN band and the lower spectrum of the X-band. The experimental radiation patterns are omnidirectional in the H-plane and bidirectional pattern in the E-plane. The proposed antenna is fabricated, and experimental results are verified on a vector network analyzer.

Keywords: Simple Iterative; Fractal, Parasitic; Pentagon; Notch band; Wide band.

doi: https://dx.doi.org/10.3329/jsr.v17i2.74173 J. Sci. Res. **17** (2), 377-391 (2025)

1. Introduction

The fractal antennas have received great attention in ultrawideband (UWB) communication due to their merits such as wideband characteristics, planar structure, miniaturized compact size and multiband operation. The latest advancement in the field of wireless communication has more exposure towards the development of miniaturized and compact wireless gadgets. Such compact wireless gadgets also need antennas with multiband operation characteristics to cater multiple wireless communication services. These characteristics are achieved by unique features of fractal geometry such as self-similarity and space filling properties [1-3]. A self-similar consists of its scaled down copies. Each

* *Corresponding author*: shinde.pratap07@gmail.com

scaled down element of antenna geometry initiates a new resonant frequency with increase the electrical length of the antenna and give rise multiband operation characteristics [4, 5]. The space filling property of fractals with more number of iterations shown miniaturisation of antenna size with increase in electrical lenghth. The fractal geometries and iterated function system (IFS) based on application of a series of affine transformation has been used to generate a fractal structure [6,7]. The design of CPW feed monopole antenna is demonstarted with circular and rectangular fractal shape radiator element [8]. Fractal antennas are preferred because they have extreme wide bandwidth. In [9] the design of planar monopole antenna using the Penta-Gasket-Koch (PGK) is discussed for wideband of 18.5 GHz.

The octal shaped fractal UWB antenna has been reported with wide impedance bandwidth of 11.42 GHz and peak gain of 3.78 dBi [10]. The wheel shape fractal antenna exhibits wide bandwidth characteristics with antenna miniaturization [11]. The CPW feed has found advantages in comparison with coaxial feed concerned with bandwidth enhancement. The CPW feed pentagonal-cut fractal antenna discussed [12] bandwidth enhancement of 12.5 GHz with peak gain of 3.4dBi. The UWB fractal antennas discussed above has been reported with arge physical dimension and fractal geometry based on self-similarity and space-filling property. The integration of such wideband antennas with monolitheic microwave integrated circuits is bit difficult due to their large dimension [13,14] and they can not be used in domastic indoor wireless communication devices. Gurpreet *et al*. [15] designed a multiband nested square shaped ring fractal antenna with circular ring elements for wireless communication applications. This antenna is useful for the operation in LTE 2300/LTE 2500, Bluetooth, WLAN, WiMAX, ITU bands. Shobit *et al*. and Rania *et al*. [16,17] presented circular ring fractal ring antenna designs for SHF and UWB applications.

These reported antennas are designed on a costly Rogers RT-5880 substrate with large dimensions and dielectric constant of 2.2. The particle swarm optimization technique is demonstrated [17] to achieve UWB operation without miniaturization of antenna size. Fractal geometry offers wideband and multiband operation. MIMO fractal antenna with hexa slot wheel shaped fractal geometry is developed and presented [18] for UWB application. Such antenna design geometry is complex due to use of six iterations to achieve wide bandwidth. Also star shaped fractal slot antenna design [19] with large dimension of 100 mm × 110 mm for dual narrow band operation with low gain of 1.058 dBi is not worth. It is advantageous to use space filling properties while designing fractal antenna geometry for size reduction. For miniturization more number of iterations scale down the geometry and increases the electrical length of the antenna. On the other side it is observed that more number of iterations increase the complexity of the antenna structure, which leads to occur fabrication error. An increase of the dielectric substrate properties like effective permittivity and permeability produce miniaturization antenna.

Though the CPW feed offers the advantage of wide bandwidth, microstrip feed ectromagnetically coupled pentagonal parasitic patch antenna demonstarted wide bandwidth of 4.21 GHz and gain 4.24dBi for wireless applications [20]. Designs with

microstrip feed monopole pentagonal shape UWB antenna loaded with slot in radiating patch and parasitic resonator on back side of RO3003 substrate has been reported and investigated for triple notch band operation [21]. Zitong *et al*. [22] demonstrated the five notch band compact antenna design for the IoT and wireless communucation with very moderate gain. It has been shown [23] that the use one semicircular split ring resonator EBG structures in cup shaped monopole antenna can help to achieve dual band notch characteristics to avoid the interference of Wi MAX and WLAN.

The author shows design of a dual-band optical imaging system-integrated patch antenna of size 100 mm × 100mm, based on an anisotropic fractal for earth observation Cube Sats [24]. Despite the simple design and necessary 1 U Cube Sat large dimension the antenna peak gain of 4dBi is not sufficient for space communication. The researchers [25] proposed an efficient broadband fractal antenna with five iterations to improve the bandwidth of the antenna of 4.3 GHz and peak gain of 6 dBi for WiMAX and WLAN applications.

In a study by Wang *et al*. [26], novel multiband fractal antennas presented with maximum gain of 3.34 dBi, which covers wireless applications such as WCDMA, LTE 42, WiMAX and WLAN. The researchers of [27] designed and discussed a compact and novel microstrip quad patch triple band Yadi-Uda alike antenna suitable for 5G/6G mobile communication in K band. In literature [28], a dual band antenna structure for the satellite and 5G communication is discussed using cross flower shaped fractal geometry. The antenna based on crossed floral square-shaped split-ring resonators organized in a Minkowski fractal configuration increases the dimension of antenna 70 × 74 mm^2. The split-ring resonators elements remove maximum copper from the top side of substrate, which resulted into poor gain of 2.05dBi. The narrow band wireless communication systems, such as IEEE 802.11a WLAN, and HIPERLAN/2, are operating in the range of 5-6 GHz.

It is observed that most of the fractal antennas design reported with large dimensions of substrate and radiating patch. Also, these reported antennas use more fractal iterations for wideband generation. The greater number of iterations increase the complexity of the antenna which causes antenna fabrication errors. Also Multiband antennas reported possess narrow bandwidth. These antennas design demonstrated with low peak gain. While designing multiband antenna it is essential to consider coexistence of narrow band services like WiMAX and WLAN across wide band. Instead of designing multiple notch bands, it is worthy to design UWB fractal antenna with a wide band-notch filter, which rejects interference of closely associated existing narrow bands services. Therefore, there is need to design an antenna which will overcome the research gap as discussed above.

In this paper a novel simple iterative pentagonal shaped compact fractal antenna design is proposed with dual wide band-notched characteristics and triple wide band operation. In first step of methodology the wide bandwidth antenna design using pentagonal fractal geomety is presented along with parametric analysis. The second step of methodology demonstrates the printing of pentagon sahped parasitic patch on back side of substrate as notch filter. The novelty of this single parasitic patch is that, it generates dual notch bands

acorss UWB band to avoid the potential interference of existing narrow bands services. The use of electromagnetically coupled pentagon sahped parasitic patch as filter is the novelty of proposed antenna. The paper is concluded with discussion on results and analysis of proposed antenna and its comparative study.

2. Methodology

The methodology used to develop the proposed fractal antenna is well explained by flowchart shown in Fig. 1. The antenna specification, optimization process, fabrication and testing are the main stages. The pentagon is inscribed in a circle with a side length *S* which is calculated from effective radius of circle. The dominant mode resonant frequency f_r of circular patch is given by Eq. (1).

$$f_{r(110)} = \frac{1.8412\ \vartheta_0}{2*\pi*a\sqrt{\varepsilon_r}} \quad (1)$$

Where $\vartheta 0$ is free space velocity, '*a*' is radius of circular patch and ε_r is dielectric constant of FR4 substrate. The radius a is given by Eq. (2)

$$a = \frac{F}{\left\{1+\frac{2h}{\pi*F*\epsilon_r}\left[\ln\left(\frac{\pi F}{2h}\right)+1.7726\right]\right\}^{1/2}} \quad (2)$$

where, *h* is height of substrate, and *F* is given by Eq. (3)

$$F = \frac{8.791*10^9}{f_r\sqrt{\epsilon_r}} \quad (3)$$

The effective radius of the antenna is given by Eq. (4)

$$a_e = a\left\{1+\frac{2h}{\pi*a*\epsilon_r}\left[\ln\left(\frac{\pi a}{2h}\right)+1.7726\right]\right\}^{1/2} \quad (4)$$

The side length of the pentagon '*S'* is calculated from effective radius by Eq. (5) considering central angle $\theta=72^0$

$$S = 2*\ a_e*\ \sin(\theta/2) \quad (5)$$

2.1. *Development of simple iterative wideband antenna*

The proposed antenna design is based on fundamental pentagon shaped radiating patch. The initial resonant frequency is determined using Eq. (1) to Eq. (4). The side length of pentagon is calculated using Eq. (5). The geometric structure of the simple iterative antenna is shown in Fig. 1. Fig. 2(a) demonstrates the progressive development stages of radiating patch of antenna, while Fig. 2(b) shows the specific geometry of the proposed antenna with three iterations. The CPW feed line is used to feed antenna. The antenna radiating copper patch is indicated by the black-color, whereas the non-metallic part is represented by the white area. This antenna is fabricated on a 1.6 mm thick FR4 substrate with a dielectric constant of 4.4 and a tangent loss of 0.02. The FR4 material is used for antenna fabrication because it is flame retardant and withstands temperatures above 345 °C. FR4 does not absorb the water. It possesses high mechanical strength and retains its excellent electrical insulating properties in both dry and humid environment. Antenna performance is not sensitive to humid environment. As the number of iterations increases, the electrical length of the antenna increases. The insertion of triangular slots in the antenna geometry generates

discontinuities along the current path. This slotted structure plays a vital role in generating self-reactance and forming traps to storage energy. The CAD model of the proposed antenna is simulated using high frequency structure simulator (HFSS). HFSS is a 3D electromagnetic tool, which uses the finite element method, used to simulate high frequency antenna.

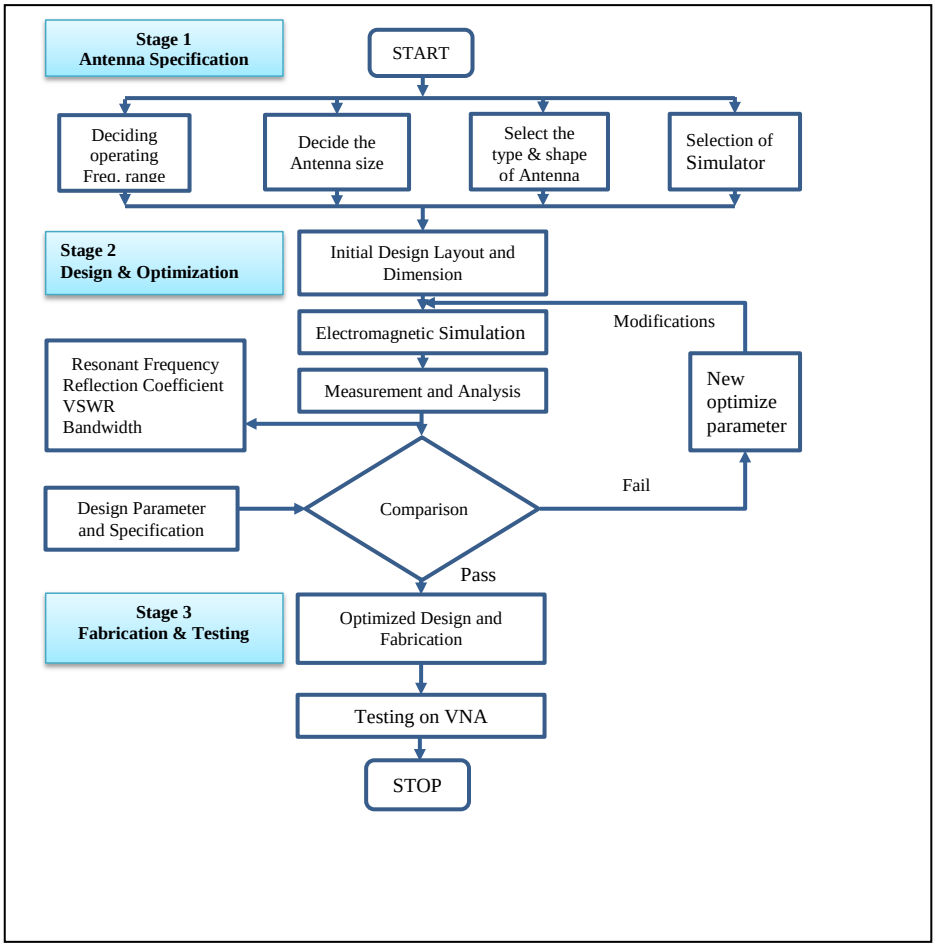

Fig. 1. Flowchart of antenna design process.

(a)

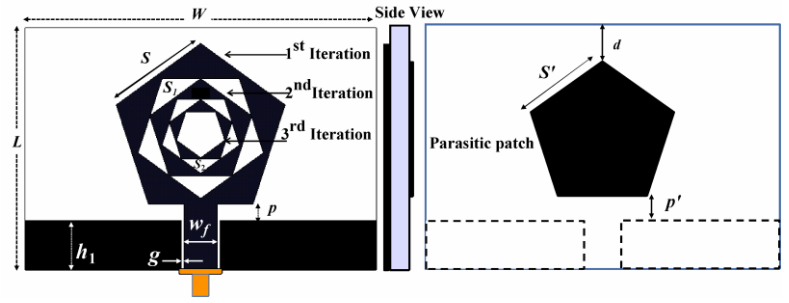

(b) (c)

Fig. 2. (a) Development of Iteration (b) Pentagon radiating patch with three iteration (c) Parasitic patch on bottom side of substrate.

2.2. *Parametric analysis*

In the simulation, the signal is connected to the radiating patch of the antenna via a wave port. To ensure impedance matching, various antenna dimensions such as the coupling gap (g), distance between the ground and patch (p), feed width (w_f), and side length of the iteration patch (S) are finely tuned. Fig. 3(a) shows the effect of the variation in feed width on reflection coefficient of antenna. The parametric analysis of the feed width is very important to match the characteristics impedance of feed line to 50 ohm and hence the impedance of the radiating patch. It is observed that maximum energy is radiated at feed width w_f = 2.8 mm as compared to 2.6 and 3 mm. But the optimum value of the feed width w_f = 3mm is chosen as it increases the bandwidth. Fig. 3(b) depicts a comparative study, indicating that by fine-tuning the ground height (h_1) and parameter (p) results into good impedance matching with wide impedance bandwidth. The Poor impedance matching is observed at p = 2.446 mm and ground height h_1 = 3.5 mm. A wide bandwidth of 4.758 GHz (2.94 –7.698) cantered at 3.5 GHz is noted at p = 0.446 mm and h_1 = 5.5 mm. The optimal values of p = 1.446 mm and h_1 = 4.5 mm yield an -10 dB impedance bandwidth of 8.73 GHz (ranging from 2.78 GHz to 11.51 GHz) and a return loss of -43.3 dB for the third iterative antenna. The measured 10 dB wide impedance bandwidth is in agreement with the simulation results. The smith chart shows in Fig. 3(c) 50 Ω impedance matching over the entire wide bandwidth of 8.73 GHz.

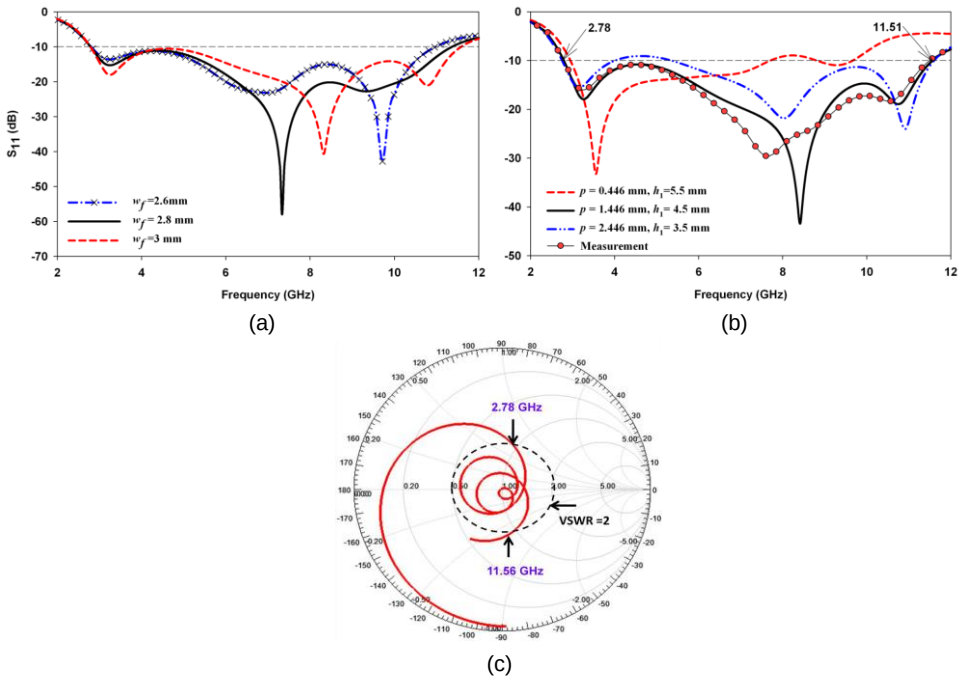

Fig. 3. (a) Reflection coefficient of iterative antenna (b) parametric analysis of antenna with variation in p and h_1 (c) Impedance matching across wide band VSWR <2.

2.3. *Design of fractal band notch antenna*

The pentagonal-shaped parasitic notch patch is etched on the bottom plane of the substrate, as illustrated in Fig. 2(c), which is used as notch filter. This filter patch is electromagnetically couple with the fractal radiating patch. The optimal parameters for the band-notched antenna are as follows: W = 32 mm, L = 22 mm, h_1 = 4.5 mm, w_f = 3.0 mm, g = 0.5 mm, p = 1.446 mm, S = 9.522 mm, S_1 = 5.903 mm, S_2 = 3.658 mm, d = 3 mm, p' = 1.113 mm, and S' = 8.699 mm. The parameters p', d, and S' play a vital role in tuning the notch frequency across the 8.73 GHz bandwidth to avoid the potential interference of existing narrow bands. The side length S' of the electromagnetically coupled pentagonal shaped parasitic patch, is optimized to 8.699 mm, which is approximately 0.913 times the side length of the radiating patch's first iteration, S = 9.522 mm. This side length of the parasitic patch is chosen to be approximately a quarter of the guided wavelength (λg/4), calculated at 5.24 GHz within the WLAN 802.11a band. In this design, the guided wavelength, λ_g, is determined using Eq. (6). Where, λ_0 represents the free space wavelength. The effective permittivity, ε_{eff}, is given by Eq. (7). It is observed that notch bands created at 5.6 GHz, 9.3 GHz and 12.5 GHz depends on side length of parasitic patch and its position on backside of substrate plane. The optimized parameters of the proposed antenna are tabulated in Table 1.

$$\lambda_g = \lambda_0 / \sqrt{\varepsilon eff} \quad (6)$$

$$\varepsilon_{eff} = (\varepsilon_r + 1) / 2 \quad (7)$$

Table 1. Optimized parameters of the proposed fractal antenna using parasitic patch (in Millimeters).

W	L	w_f	h_1	G	p	p'	d	S	S'	S_1	S_2
22	32	3	4. 5	0.5	1.446	1.113	3	9.522	8.699	5.903	3.658

The layout and artwork of antenna based on optimized parameters tabulated in Table 1 is prepared by exporting .dxf CAD file from HFSS simulator to corel draw software. The positive and negative film of the antenna structure is developed to perform itching process. The copper surface of double side FR4 substrate is made free from dust and grease using zero number sand paper. The photo resist spray, known as positive-20, is used to cover up the copper surface plate of FR4 substrate for further chemical development process. The positive film of antenna structure is exposed using photo-lithographic method to develop antenna structure. The unwanted copper region of the conducting layer is precisely removed by Photo-lithographic chemical etching method.

3. Results and Discussion

Fig. 4 depicts the simulated and measured reflection coefficient S_{11} of the proposed simple iterative band-notch antenna, using electromagnetic coupled parasitic notch filter. This notch filter split wide bandwidth of 8.73 GHz the simple iterative antenna into three operating bands.

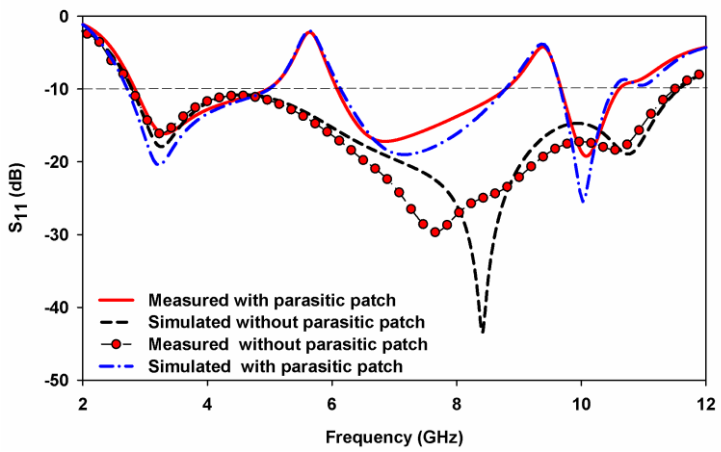

Fig. 4. Simulated and Measured reflection coefficient of the band-notched antenna

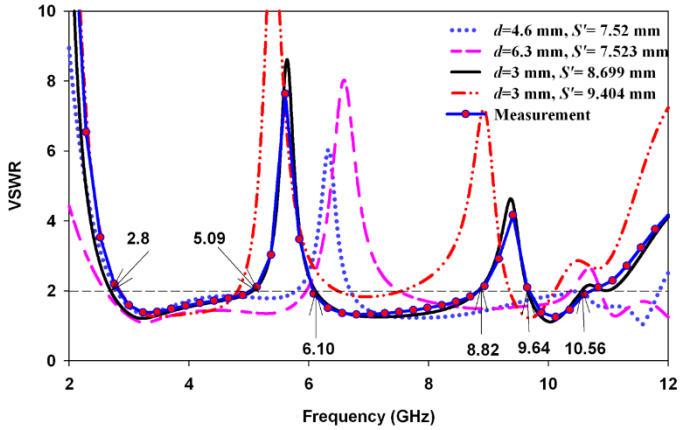

Fig. 5. Simulated and Measured VSWR of fractal band notched antenna.

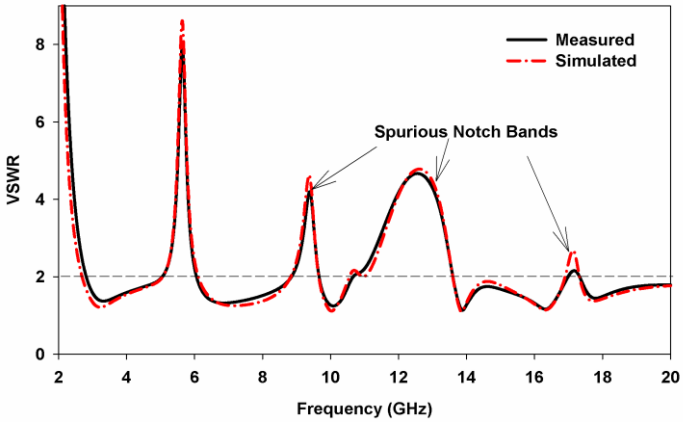

Fig. 6. Spurious notch band generated at 9.3 GHz, 12.5 GHz, and 17 GHz.

The measured lower edge frequency of the first operating band is 2.80 GHz, while the higher edge frequency of the third operating band is 10.56 GHz. The measured -10 dB impedance bandwidths of the three operating bands are 2.29 GHz (2.8 GHz to 5.09 GHz), 2.72 GHz (6.10 GHz to 8.82 GHz), and 0.92 GHz (9.64 GHz to 10.56 GHz), respectively. The first notch band, observed at 5.6 GHz.

The increase in side length S' of the parasitic patch controls the dimension parameters *p*' and *d*. With increase in S', fully covers the pentagonal fractal radiating patch and overlaps with the CPW ground plane. It leads to impedance mismatch in the CPW feed. To control the position of the notch frequency, optimizations are performed on *S*', *d*, and *p*'. At optimal values of *S*' = 8.699 mm, *d* = 3 mm, and *p*' = 1.113 mm, a VSWR > 2 notch bandwidth of 1.01 GHz (5.09 GHz to 6.10 GHz), centered at 5.6 GHz, is achieved, as shown in Fig. 5.

The notch band effectively rejects the WLAN 802.11a band centered at 5.24 GHz. Furthermore, by tuning the dimensions of *d*, *S*, and *p*', the band-notch frequency can be shifted to 5.6 GHz. The notch band centered at 9.3 GHz, with a bandwidth of 0.82 GHz (8.82 GHz to 9.64 GHz), rejects the lower spectrum of X-band applications. The three spurious notch bands occur at 9.3 GHz, 12.5 GHz, and 17 GHz as shown in Fig. 6. The spurious notch band generated at 12.5 GHz exhibits a rejection bandwidth of 3 GHz (10.6 GHz to 13.6 GHz). The performance of proposed pentagonal shaped fractal antenna without and with band notch is summarized in Table 2. The variation is simulated and a measured result is negligible. The minor errors may be caused due to long itching time taken during fabrication process, which causes loss in conductive layer on substrate.

Table 2. Performance of proposed antenna pentagonal shaped fractal band notch antenna.

Antenna type	Band 1		Band 2		Band 3	
	BW (GHz), (f_1- f_2)		BW (GHz), (f_1- f_2)		BW (GHz), (f_1- f_2)	
	Simulated	Measured	Simulated	Measured	Simulated	Measured
Fractal wideband antenna	8.78 2.80–11.58	8.73 2.78–11.51	------	------	------	------
Fractal band notch antenna	2.3 2.70–5.00	2.15 2.81–4.96	2.66 6.14–8.8	2.71 6.07–8.78	0.86 9.65–10.51	0.94 9.67–10.61

3.1. *Antenna radiation characteristics*

The radiation pattern in the E-plane and H-plane with co and cross-polarization is illustrated in Fig. 7. In Fig. 7(a), it is observed that the antenna possesses bidirectional radiation characteristics in the E-plane at 3.2 GHz, 7.1 GHz, 10GHz and 15GHz. The cross-polarization observed is very less. At 10 GHz and 15 GHz, side lobes are generated, indicating a lower radiation and hence gain in the broadside direction. The radiation pattern at 15 GHz reveals that the antenna exhibits good radiation at $\varphi = 0°$ and $\theta = 300°$. This directional characteristic could be attributed to edge reflections. Fig. 7(b) shows H-plane radiation patterns at various resonant frequencies, which are omnidirectional at both lower and higher frequencies.

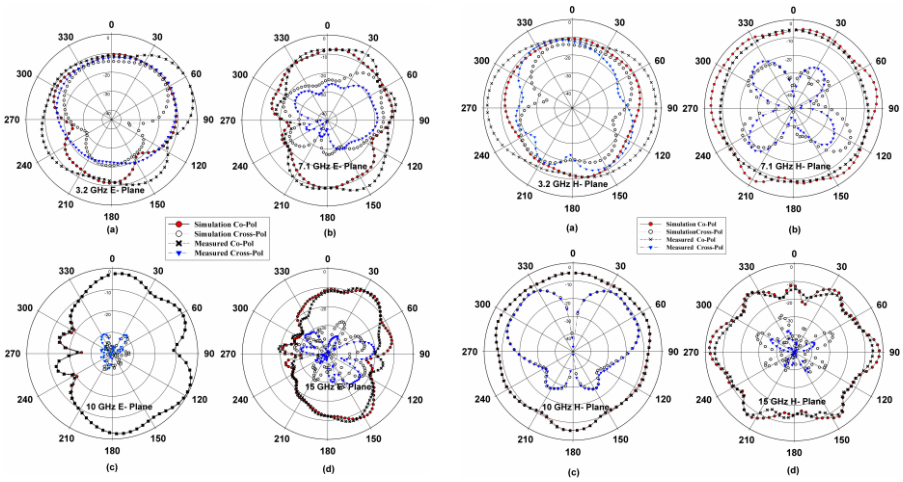

(a) (b)

Fig. 7. Simulated and measured radiation pattern 3.2GHz, 7.1 GHz, 10 GHz, 15 GHz (a) E-plane (b) H-plane.

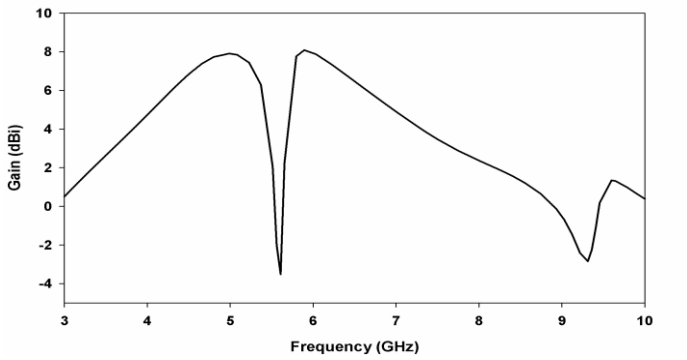

Fig. 8. Gain of proposed fractal band-notched antenna.

The antenna exhibits a maximum gain of 8 dBi over the operating bands, as shown in Fig. 8. However, the gain decreases at the rejected frequencies as expected. Fig. 9(a) and Fig. 9(b) shows the current distributions along the edge of radiating patch, while, Fig. 9(c) and Fig. 9(d) shows current distribution at both notch frequencies. At first notch frequency 5.6 GHz the maximum current is accumulated on encircled opposite side length of parasitic patch as shown in Fig. 9(c), which individually operates at quarter wavelength of center rejection frequency. At second notch frequency 9.3 GHz the maximum current is concentrated on upper adjacent side length of parasitic patch, which individually operates at half wavelength of center rejection frequency as shown in Fig. 9(d). The fabricated prototype of proposed antenna is shown in Fig. 9(e). The antenna dimensions are in mm and very small. Hence the minor difference in simulated and measured results is due to antenna

fabrication process. Also, the very less measurement errors as man made errors are introduced in alignment of antennas during measurement. Overall, the measured and simulated results are in good agreement.

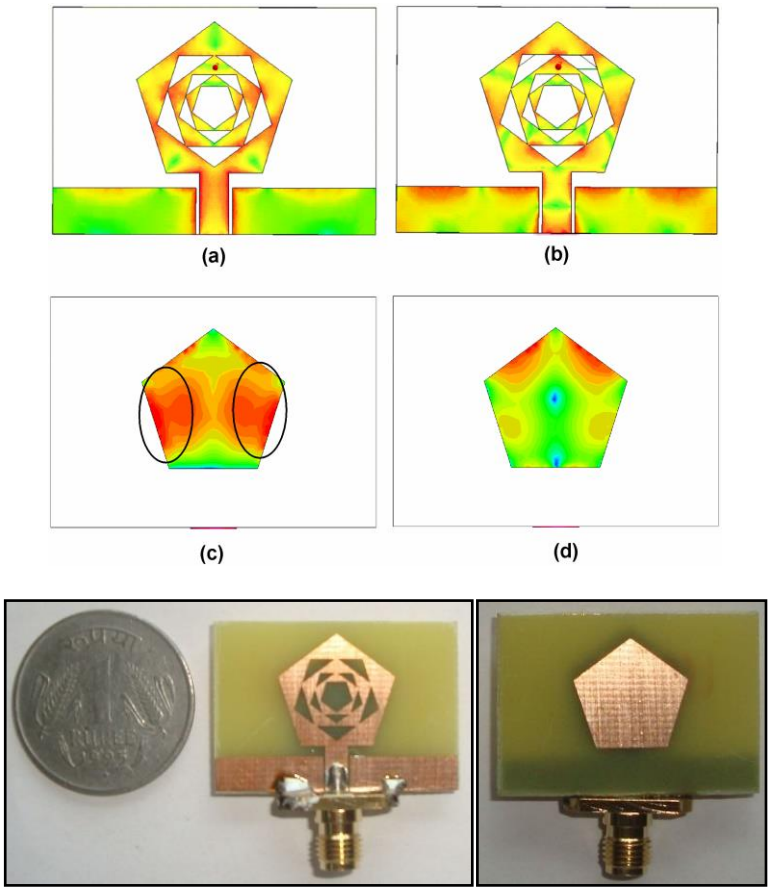

(e)

Fig. 9. Simulated current distribution at (a) 10 GHz (b) 14 GHz (c) notch frequencies 5.6 GHz (d) 9.3 GHz (e) Fabricated pentagonal shaped fractal band notch antenna.

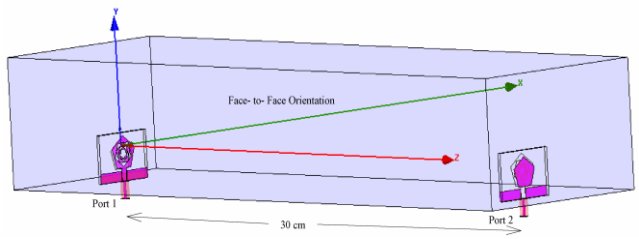

(a)

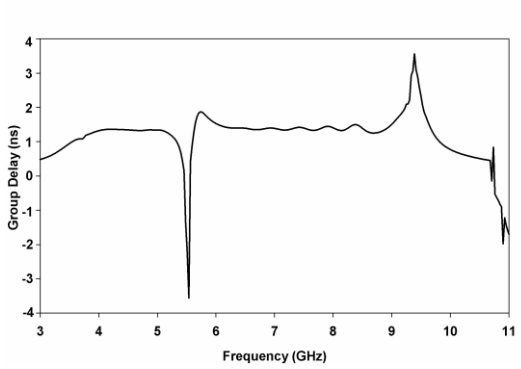

(b)

Fig. 10. (a) Group delay measurement set up (b) Group delay of antenna.

The group delay of proposed antenna is measured far field. The simulation set up for measurement of group delay using HFSS simulator is shown in Fig. 10(a). Pair of identical pentagonal fractal antennas is separated by a distance of 30 cm in the far field with face to face orientation. The group delay observed is shown in Fig. 10(b). It is observed that the group delay variation of the fractal antenna is less than 1ns over the operating band, except at the notch-band. Constant group delay indicates linear phase. The performance comparative study of proposed antenna with past reported antenna design is tabulated in Table 3. The dimension of proposed antenna is comparatively small with reference to past reported antennas.

Table 3. Comparison of proposed antenna with past reported antennas.

Refs.	Antenna Size (mm^2)	Structure technique used	No of iterarions, Reso. band	S_{11} (dB)	Resonating frequency range, Impedance BW(GHz)	Peak gain (dBi)
[11]	90 × 80	CPW Wheel Shape Fractal	05, 1	–14	0.95 - 4.495, 3.545	3.79
[12]	58 × 52.45	Pentagonal-Cut Fractal	05, 1	–48	2.5 – 15, 12.5	----
[15]	36 × 32	Microstrip feed Nested Square Shaped Ring Fractal	3, 5	–38	3.23 GHz	2.5
[18]	40 × 45	Hexa-Slot Wheel Shaped Fractal Orthogonal MIMO	6, 1	–46	1.29–15.09, 13.8	3.2
[17]	38 × 45	Circular Ring-Shaped UWB Fractal	4, 1	–40	2.05–14.5, 12.45	6.0
[19]	112 × 100	A Dual Band Star-Shaped Fractal Slot	3, 2	– 24.6 – 23.9	> 0.1	1.058.0
[24]	100 × 100	Patch Antenna Based on an Anisotropic Fractal	2, 2	–17 –36	2.35–2.48, 0.13 2.01– 2.05, 0.04	-1 2.15
[26]	87.5 × 61	Novel Multiband Fractal	4, 3	–14 –27	1.8–2.9, 1.1 3.4–4.6, 1.2	2.98 2.58

				–30	5–5.6, 0.6	3.34
[28]	70 × 74	Crossed Flower Shaped Fractal	5, 2	–35 –50	4.01–4.82, 0.81 7.6–7.94, 0.34	1.5 2.05
Prposed Fractal Antenna	32 × 22	Pentagonal shaped parasitic patch and fractal antenna	3, 3	–17 –18 –20	2.81–4.96, 2.15 6.07–8.78, 2.71 9.67–10.61, 0.94	8.0

4. Conclusion

In this study, two different pentagonal-shaped fractal antennas with and without band notch using electromagnetically coupled parasitic patches are proposed and investigated. The impedance bandwidth of the proposed antenna is enhanced to 8.73 GHz, compared with its single iteration design. The electromagnetically coupled parasitic patch as a notch band filter is the novelty of the presented work. The wide fractional bandwidth of 122.18 % is chopped into three operating bands by a pentagon-shaped parasitic band-notch filter. The measured fractional bandwidth of three operating bands resonating in the vicinity of 3.2 GHz, 7.1 GHz, and 10 GHz is 64.60 %, 36.49 %, and 9.27 %, respectively. The wide notch bands centered at rejection frequencies of 5.6 GHz and 9.3 GHz avoid the potential interference of the entire 802.11a WLAN system and lower X-band applications. The omni-directional radiation pattern is achieved over the operating bands in the H-plane and a bidirectional pattern in the E-plane. The small dimension of the proposed antenna with a peak gain of 8dBi is a good candidate for wireless applications.

References

1. D. H. Werner and S. Ganguly, IEEE Antennas Propag. Magaz. **45**, 38 (2003). https://doi.org/10.1109/MAP.2003.1189650
2. J. P. Gianvittorio and Y. Rahmat-Samii, IEEE Antennas Propag. Magaz. **44**, 20 (2002). https://doi.org/10.1109/74.997888
3. S. R. Best, IEEE Antennas Wirel. Propag. Lett. **1**, 22 (2002). https://doi.org/10.1109/LAWP.2002.802579
4. K. C. Hwang, IEEE Antennas Wireless Propag. Lett. **6**, 357 (2007). https://doi.org/10.1109/LAWP.2007.902045
5. N. Bayatmaku, P. Lotfi, M. Azarmanesh, and S. Soltani, IEEE Antennas Wirel. Propag. Lett. **10**, 873 (2011). https://doi.org/10.1109/LAWP.2011.2165195
6. S. R. Best, IEEE Antennas Wirel. Propag. Lett. **2**, 197 (2003). https://doi.org/10.1109/1-AWP.2003.819680
7. P. W. Tang, Proc. IEEE Antennas Propag. Soc. Int. Symp. **4**, 230 (2003). https://doi.org/10.1109/APS.2003.1220162
8. Y.-C. Lee, J.-S. Sun, and S.-C. Lin, Microw. Opt. Technol. Lett. **49,** 1267 (2007). https://doi.org/10.1002/mop.22448
9. M. Naghshvarian-Jahromi, IEEE Trans. Antennas Propag. **56**, 3844 (2008). https://doi.org/10.1109/TAP.2008.2007393
10. J. P. Shinde, R. Kumar, P. Shinde, and M. D. Uplane - *In Proc. of IEEE Conf. Appl. Electromag*. (2009). https://doi.org/10.1109/AEMC.2009.5430719
11. R. Kumar, P. Malathi, and K. Sawant, Microw. Opt. Technol. Lett. **53**, 155 (2011). https://doi.org/10.1002/mop.25677
12. R. Kumar and P. N. Chaubey, IET Microw. Antennas Propag. **6**, 1407 (2012). https://doi.org/10.1049/iet-map.2011.0188

13. A. Azari and J. Rowhani, Prog. Electromag. Res. **2**, 7 (2008). https://doi.org/10.2528/PIERC08031005
14. A. Azari, IEEE Trans. Antennas Propag. **59**, 1724 (2011). https://doi.org/10.1109/TAP.2011.2128294
15. G. Bharti and J. S. Sivia, Prog. Electromag. Res. C **108**, 115 (2021). https://doi:10.2528/PIERC20110601
16. S. Agarwal and Umair, Prog. In Electromag. Res. C **134**, 53 (2023). https://doi:10.2528/PIERC23033110
17. R. H. Elabd and A. J. A. Al-Gburi, Prog. Electromag. Res. B **106**, 101 (2024). https://doi:10.2528/PIERB24033002
18. R. Deshpande and U. Yalavarthi, Prog. Electromag. Res. Lett. **116**, 31 (2024). https://doi:10.2528/PIERL23110301
19. R. Malallah, R. M. Shaaban, and W. A. G. Al-Tumah, Int. J. Electron Commun. **127**, 1 (2020). https://doi.org/10.1016/j.aeue.2020.153473
20. P. N. Shinde and J. P. Shinde, AEU Elsevier Int. J. Electronics Commun. **69**, 1489 (2015). https://doi.org/10.1016/j.aeue.2015.07.001
21. A. A. Kadam, A. A. Deshmukh J. Microwaves, Optoelectronics Electromag. Applicat. **20**, 320 (2021). https://doi.org/10.1590/2179-10742021v20i21157
22. Z. Zhao, C. Zhang, Z. Lu, and G. Li, Proc. of the IEEE 10th Asia Pacific Conf. on Antenna and Propagation (Xiamen, China, November, 2022).
23. J. J. Shi, Y. Y. Wang, and J. M. Tu, Int. Appl. Comput. Electromag. Soc. Sympo. (China, 2022). https://doi.org/ 10.1109/ACES-China56081.2022.10065215
24. N. Meirambekuly, A. A. Temirbayev, Z. Z. Zhanabaev, B. A. Karibayev, T. A. Namazbayev, B. A. Khaniyev, and A. K. Khaniyeva, Ain Shams Eng. J. **13**, 1 (2022). https://doi.org/10.1016/j.asej.2021.07.010
25. M. Marzouk, I. H. Nejdi, R. Youssef, S. Barua, S. Mohamed, S. Ahmad, and M. Hussein, Heliyon **10**, 1 (2024). https://doi.org/10.1016/j.heliyon.2024.e26087
26. L. Wang, J. Yu, T. Xie, and K. Bi, Int. J. Antennas Propag. **17**, 1 (2021). https://doi.org/10.1155/2021/9926753
27. R. K Singh and K. Mamta, J. Sci. Res. **16**, 187 (2024). http://dx.doi.org/10.3329/jsr.v16i1.66715
28. U. Patel, T. Upadhyaya, V. Sorathiya, K. Pandya, A. Alwabli, K. Dave, N. F. Soliman, and W. El-Shafai, Results Eng. **22**, 1 (2024). https://doi.org/10.1016/j.rineng.2024.102110